Infection, Genetics and Evolution 91 (2021) 104815

Contents lists available at ScienceDirect

Infection, Genetics and Evolution

journal homepage: www.elsevier.com/locate/meegid

Research paper

Molecular characterization of interactions between the D614G variant of SARS-CoV-2 S-protein and neutralizing antibodies: A computational approach

Alexander Kwarteng [a,b,*], Ebenezer Asiedu [b], Augustina Angelina Sylverken [b,d], Amma Larbi [a], Samuel Asamoah Sakyi [c], Samuel Opoku Asiedu [b,d]

[a] Department of Biochemistry and Biotechnology, Kwame Nkrumah University of Science and Technology (KNUST), Kumasi, Ghana
[b] Kumasi Centre for Collaborative Research in Tropical Medicine (KCCR), Kumasi, Ghana
[c] Department of Molecular Medicine, Kwame Nkrumah University of Science and Technology (KNUST), Kumasi, Ghana
[d] Department of Theoretical and Applied Biology, Kwame Nkrumah University of Science and Technology (KNUST), Kumasi, Ghana

ARTICLE INFO

Keywords:
SARS-CoV-2
D614G
S-protein
Molecular dynamics simulation
Neutralizing antibody

ABSTRACT

The D614G variant of SARS-CoV-2 S-protein emerged in early 2020 and quickly became the dominant circulating strain in Europe and its environs. The variant was characterized by the higher viral load, which is not associated with disease severity, higher incorporation into the virion, and high cell entry via ACE-2 and TMPRSS2. Previous strains of the coronavirus and the current SARS-CoV-2 have demonstrated the selection of mutations as a mechanism of escaping immune responses. In this study, we used molecular dynamics simulation and MM-PBSA binding energy analysis to provide insights into the behaviour of the D614G S-protein at the molecular level and describe the neutralization mechanism of this variant. Our results show that the D614G S-protein adopts distinct conformational dynamics which is skewed towards the open-state conformation more than the closed-state conformation of the wild-type S-protein. Residue-specific variation of amino acid flexibility and domain-specific RMSD suggest that the mutation causes an allosteric conformational change in the RBD. Evaluation of the interaction energies between the S-protein and neutralizing antibodies show that the mutation may enhance, reduce or not affect the neutralizing interactions depending on the neutralizing antibody, especially if it targets the RBD. The results of this study have shed insights into the behaviour of the D614G S-protein at the molecular level and provided a glimpse of the neutralization mechanism of this variant.

1. Introduction

Severe acute respiratory syndrome associated coronavirus 2 (SARS-CoV-2) is the causative agent of the 2019 coronavirus disease (COVID-19), which was declared a pandemic by the World Health Organization (WHO) on March 11, 2020. The period between the latter part of February and March 2020 saw the emergence of the SARS-CoV-2 S-protein D614G variant which distributed globally after dominating Europe (Isabel et al., 2020; Korber et al., 2020). The D614G mutation is caused by a substitution of an A to G at position 23,403 of the Wuhan reference sequence resulting in the replacement of aspartate with glycine at position 614 of the S-protein (Korber et al., 2020). The S-protein is a glycoprotein attached to the viral surface, which mediates receptor binding and facilitates viral entry into host cells (Yi et al., 2020). The S-protein is comprised of the S1 and S2 subunits. The S1-subunit has three domains: N-terminal domain (NTD), C-terminal domain (CTD) and receptor-binding domain (RBD). The mechanism of neutralization of the SARS-CoV-2 by antibodies involves binding the neutralizing antibody to the RBD or NTD, with the aim of interfering interactions with human angiotensin-converting enzyme 2 (ACE-2) (Barnes et al., 2020; Piccoli et al., 2020). Previous strains of the coronavirus outbreaks and the current SARS-CoV-2 can manipulate their genomes to select mutations resistant to monoclonal antibodies or convalescent plasma (Li et al., 2020; Sui et al., 2008; ter Meulen et al., 2006).

The D614G variant has been characterized by higher viral load, which is not associated with disease severity (Korber et al., 2020; Volz et al., 2021), higher incorporation into virion (Zhang et al., 2020), and

* Corresponding author at: Department of Biochemistry and Biotechnology, KNUST, Kumasi, Ghana.
E-mail address: akwarteng@knust.edu.gh (A. Kwarteng).

https://doi.org/10.1016/j.meegid.2021.104815
Received 27 October 2020; Received in revised form 10 March 2021; Accepted 20 March 2021
Available online 24 March 2021

high cell entry via ACE-2 and TMPRSS2 (Ogawa et al., 2020; Ozono et al., 2021). The molecular features of the D614G S-protein conformational dynamics and its potential effect on the interactions with neutralizing antibodies have not been extensively looked at. In this study, we used molecular dynamics simulation and MM-PBSA binding energy analysis to provide insights into the behaviour of the D614G S-protein and describe the neutralization interactions between the variant and neutralizing antibodies. Our results show that the D614G S-protein adopts distinct conformational dynamics, which is skewed towards the open-state conformation more than the closed-state conformation of the wild-type S-protein. Residue-specific variation of amino acid flexibility and domain-specific RMSD suggest that the mutation causes an allosteric conformational change in the RBD. Evaluation of the interaction energies between the S-protein and neutralizing antibodies show that the mutation may increase, decrease or not affect the neutralizing interactions depending on the neutralizing antibody.

2. Methods

2.1. Structure preparations

The UniProt database (https://www.uniprot.org/uniprot/) was used to access the sequence of SARS-CoV-2 S protein Wuhan reference. All protein models were generated and validated using the SWISS-MODEL server (https://swissmodel.expasy.org/). The S-protein models used in this study were the D614G variant of the SARS-CoV-2 S-protein and the wild-type S-protein (closed-state and open-state). The mutation of aspartate-614 to glycine was accomplished by the PyMol mutagenesis tool (Yuan et al., 2017). The structural co-ordinates of the templates were obtained from the Protein Data Bank (https://www.rcsb.org/).

2.2. Phylogenetic analysis

The ConSurf server was used to calculate the evolutionary conservation degree of each SARS-CoV-2 S-protein residue. The server (http://consurf.tau.ac.il) provides an evolutionary profile of the amino acids, which define their level of importance to the protein's biological activity and structure. The following parameters were selected for phylogenetic analysis: homologous search algorithm: CSI-BLAST; number of iterations: 3; *E*-value cut-off: 0.0001; protein database: UNIREF-90; number of reference sequences selected: 150; maximum sequence identity: 95%; minimum identity for counterparts: 35%; alignment method: Bayesian; calculation method: MAFFT-L-INS-i; and evolutionary substitution model: best model.

2.3. Construction of S-protein-neutralizing antibody complexes

The studied molecular systems were comprised of the selected neutralizing antibodies (antigen-binding fragment, Fab) bound to the RBD or NTD of the SARS-CoV-2 S-protein (wild-type or D614G variant). The complexes were generated through the structural superposition of the templates and the generated models using the PyMol v2.4.

2.4. Details of molecular dynamics simulation

The wild-type and D614G S-protein systems were simulated using GROMACS v2021 (Abraham et al., 2015) and CHARMM36 force field (Vanommeslaeghe et al., 2010). The proteins were centered in a cubic box, placed 1 nm from the box edges and solvated with a three-point (tip3p) water model. Appropriate ions were added to the system to neutralize the molecular system electrostatically. Energy minimization was performed on the system using the steepest descent algorithm for 20,000 steps with a maximum force threshold of 100 kJ/mol/nm. Van der Waals interactions were treated with a single cut-off of 1.4 nm and long-range electrostatics were treated at a cut-off of 1.4 nm with the Particle-Mesh Ewald (PME) method with 0.168 FFT grid spacing and 4th order B-spline interpolation. Neighbour search was performed every 20 steps using the grid method with Verlet cut-off scheme. Protein and non-protein components of the system were independently coupled to v-rescale thermostat and an isotropic Berendsen algorithm for pressure coupling. The pressure was maintained by weak coupling to a reference pressure of 1 bar, with an isothermal compressibility of 4.6×10^5 bar-1. The bond lengths within the protein were constrained using the LINCS algorithm. NVT and NPT equilibrations were run for a total of 400 ps. Three independent simulations of 100 ns each were performed for all molecular systems. For MM-PBSA calculations, a total of 15 ns simulations was performed for each complex in triplicate using GROMACS v5.1.5.

2.5. Trajectory analysis and MM-PBSA calculations

In-built GROMACS tools were used for all trajectory processing including, re-centering, fitting, periodicity treatments, and concatenation of the trajectories before subjected to analysis. The molecular systems dynamics were evaluated based on properties such as root-mean-square deviation (RMSD) and root-mean-square fluctuation (RMSF). RMSD was calculated overall backbone atoms after least-squares fitting to the reference backbone, while the RMSF was calculated *per* residue after least-squares fitting to C-alpha atoms. In each case, the equilibrated structures were used as the reference structures (starting structure, $t = 0$ ns). The energy terms governing the S-protein-antibody interactions were calculated using the g_mmpbsa v5.1.2 (Kumari et al., 2014), which is based on the Molecular Mechanics with Poisson–Boltzmann Surface Area (MM-PBSA) approach. The binding energy ($E_{binding}$) of the system is estimated as;

$$E_{binding} = E_{MM} + G_{solv}.$$

where, E_{mm} represents the molecular mechanics energy terms, G_{solv} represents the solvation energy terms. It is worth noting that the entropic term (TS) is exempted from the calculation particularly due to the high computational demand. There are reports demonstrating that the net contribution of the entropic term is often minimal (Kumari et al., 2014). This is why the binding energy is designated as $E_{binding}$ instead of ΔG. The E_{mm} is made up of all bonded and non-bonded energies in the system, thus, can be expressed as;

$$E_{MM} = E_{bonded} + E_{nonbonded} = E_{bonded} + E_{vdW} + E_{elec}.$$

where E_{bonded} is the bonded interactions consisting of bond, angle, dihedral and improper interactions. $E_{nonbonded}$ represents the non-bonded interactions, which include both electrostatic (E_{elec}) and van der Waals (E_{vdW}) interactions which are calculated using a Coulomb and Lennard-Jones potential functions, respectively. The solvation energy term (G_{solv}) is expressed as:

$$G_{solv} = G_{polar} + G_{nonpolar}.$$

where G_{polar} represents polar solvation energies and Gnonpolar is the non-polar solvation energies. G_{polar}, which is the electrostatic contribution is calculated from solving the Poisson-Boltzmann equation. The non-electrostatic term of solvation energy, $G_{nonpolar}$, includes repulsive and attractive forces between solute and solvent that are generated by cavity formation and van der Waals interactions, respectively.

Molecular visualizations of protein structures were done with PyMol v2.4. All graphs and statistical analysis were performed with GraphPad Prism v9.02. A two-tailed unpaired Student's *t*-test was used to determine the statistical significance between wild-type and D614G S-protein RMSD. $P < 0.05$ was considered to be statistically significant.

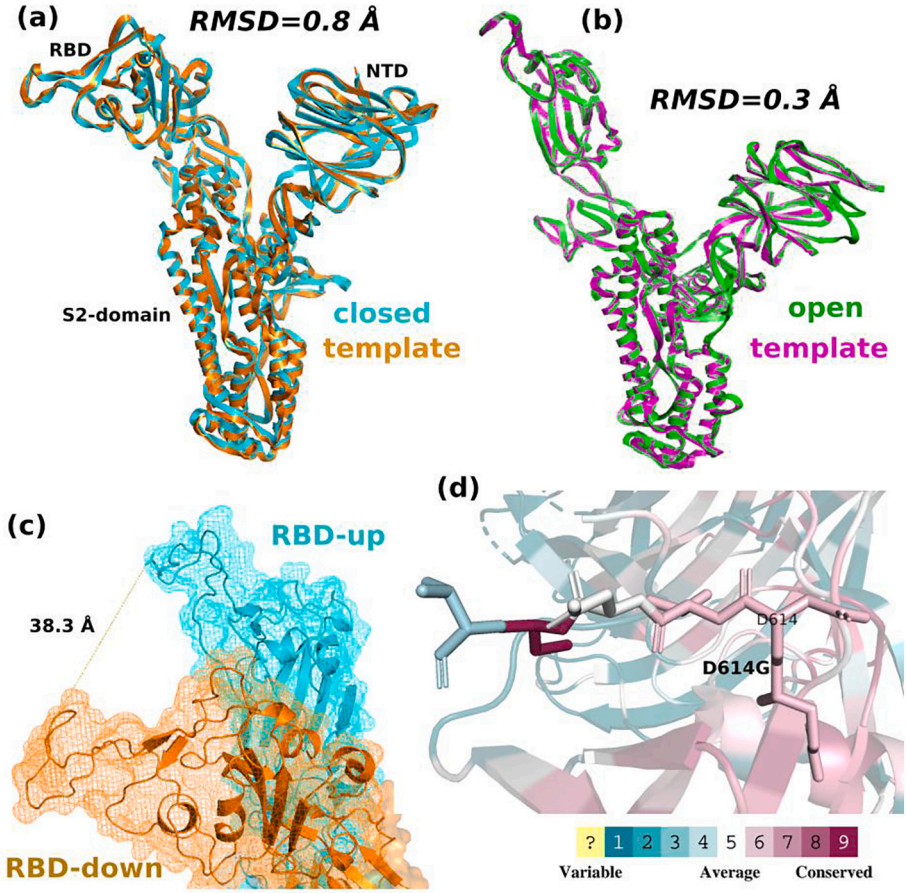

Fig. 1. Modeling of the SARS-CoV-2 S-protein. The distinct states of the S-protein were modeled based on their respective templates. Structural superposition of the (**a**) closed state to its template and **(b)** closed state to its template and their respective RMSD are show. **(c)** shows the distance the upward and downward orientation of the RBD. **(d)** shows the conservation profile of D614 of the S-protein.

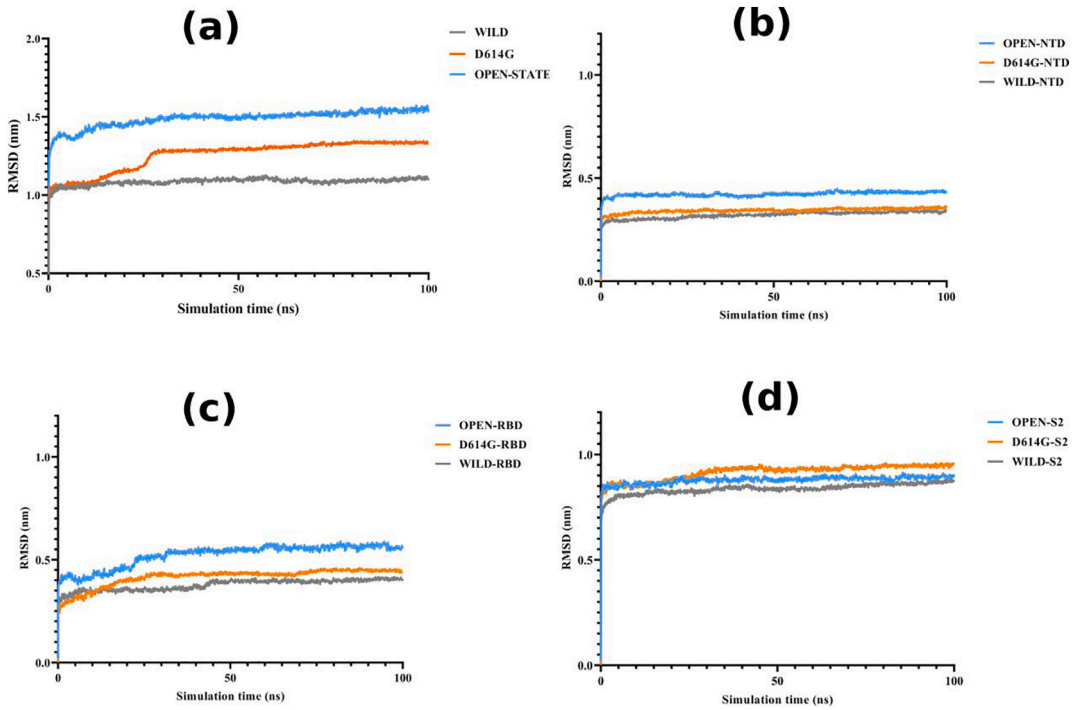

Fig. 2. Backbone-RMSD values as a function of time. (a) RMSD plot of the wild-type, D614G and open-state S-proteins. The domain-specific RMSD profiles of the (**b**) NTD (**c**) RBD and (**d**) S2-domain are also shown.

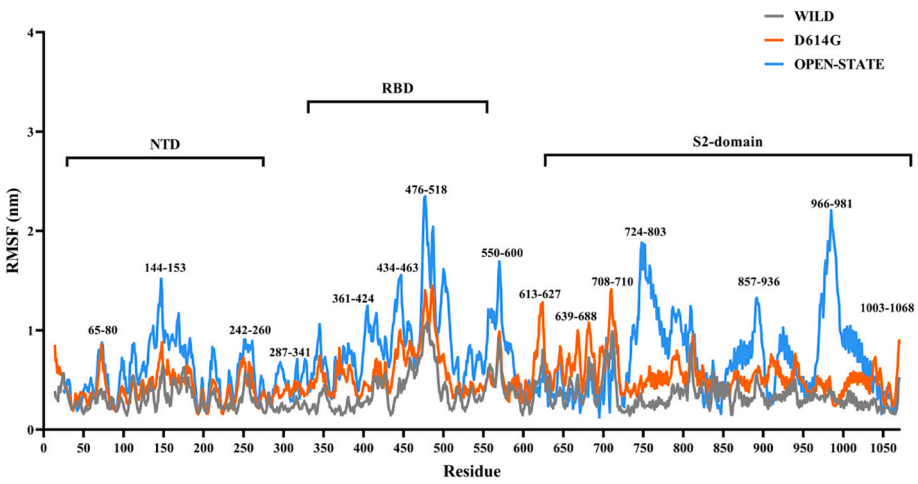

Fig. 3. RMSF profile of the protein residues during the simulation. The plot shows the residue-specific variations in amino acid flexibility and movement during the simulation. Most affected regions of the S-protein with respect to RMSF variations are shown.

3. Results

3.1. SARS-CoV-2 S-protein model

The crystallographic structures of SARS-CoV-2 S-protein at the PDB are averaged models of the resolved protein in solutions, and these structures may lack some fragments and residues (Deller and Rupp, 2015). Accordingly, we used SWISS-MODEL to generate complete structural models of both the closed-state and open-state conformations of wild-type S-protein using their corresponding templates. The closed-state and open-state of the SARS-CoV-2 S-proteins were built based on the structure of PDB ID: 7JJI and PDB ID: 7CAI, respectively. Structural superposition of the model and the templates showed that the structures are highly similar with RMSD of 0.8 Å for the closed-state model and 0.3 Å for the open-state model (Fig. 1a and b). The closed-state of the SARS-CoV-2 S-protein is characterized by the downward orientation of the receptor-binding domain (RBD down). The RBD, is oriented upwards in the open-state to be accessible for ACE-2 binding (RBD up). Structural superposition of the two distinct states of the S-protein shows that the RBDs are 38.3 Å apart (Fig. 1c).

The potential effect of the mutation was first describe using ConSurf, a tool that provides the evolutionary conservation profile of the protein residues. ConSurf identifies the residues that have importance for the overall protein structure dynamics and functions (Ashkenazy et al., 2016). There is evidence supporting the correlation between residue evolutionary conservation and protein function, such that amino acids that evolve slowly or highly conserved are important for biological activity (Liu et al., 2017). Phylogenetic analysis and multiple sequence alignment studies reveal that most residues of the S-protein are less conserved compared to other structural proteins of SARS-CoV-2, such as the nucleocapsid and membrane proteins (Kaushal et al., 2020; Ngoi et al., 2020). These low conserved residues may be frequently mutated to enhance the escape mechanism adopted by the virus. The residue conservation analysis revealed that aspartate-614 (D614) is a moderately conserved residue with ConSurf score of 6 (Fig. 1d), suggesting an important role for the residue in the biological activity and dynamics of the S-protein.

3.2. Effect of the mutation on S-protein structural dynamics

The structural impact of the mutation was studied through all-atom molecular simulation of the S-protein. The root-mean-square-deviation (RMSD) and root-mean-square-fluctuation (RMSF) were used to assess the dynamics of the S-protein. The RMSD represents the conformational stability of the protein system during the simulation because it reflects the average displacement of backbone atoms in the protein structure with reference to the starting structure (equilibrated structure, $t = 0$ ns). We have also used the RMSD parameter to decide the similarities or differences between the wild-type, D614G and open-state S-proteins.

The RMSD evolution of the molecular systems during the simulations is shown in Fig. 2a. According to the RMSD plot, convergence was reached for all molecular systems after 0.2 ns. The average RMSD values of the wild-type and D614G S-proteins were 1.09 ± 0.04 nm and 1.26 ± 0.1 nm, respectively. There was a significant difference ($p < 0.05$) in the structural similarity and conformational stability of the wild-type and D614G S-proteins. We have also shown the RMSD evolution profile of the open-state S-protein. Several studies have suggested that the D614G S-protein adopts a conformation similar to the open-state (Mansbach et al., 2020; Yurkovetskiy et al., 2020a). To further understand the structural similarities of the D614G S-protein and the wild-type conformations, we studied the domain-specific conformational stability by computing the RMSD evolution of each S-protein domain. This is important, considering that the interactions between the S-protein and neutralizing antibodies are domain-dependent. Monitoring the impact of the mutation on the conformational stability of the S-protein domains could help the study of the interaction between the virus and neutralizing antibodies. The RMSD evolution of the NTD, RBD and S2-domain were computed for the wild-type, D614G and open-state S-proteins (Fig. 2b-2d). The domain-specific RMSD for the NTD, RBD and S2-domain ranged from 0.32–0.42 nm, 0.34–0.42 nm and 0.83–0.91 nm, respectively. This suggest that the NTD and the RBD have lower conformational stability than the S2-domain in all the protein systems. The NTDs of the wild-type and D614G S-proteins have similar RMSD evolution profile (Fig. 2b). Among the domains, the NTD is expected to be the least affected by the D614G mutation since the site of variation is within the CTD. The open-state NTD showed higher RMSD (0.42 ± 0.16 nm) than the NTD of both the wild-type (0.32 ± 0.02 nm) and the D614G variant (0.34 ± 0.02 nm). The average RMSD values for the wild-type and D614G RBD were 0.38 ± 0.03 nm and 0.34 ± 0.05 nm, respectively. As shown in Fig. 2c, the RBD for the wild-type and D614G S-proteins have lower conformational stability than the open-state RBD. The S2-domain of the D614G S-protein showed the highest RMSD compared to the wild-type and open-state (Fig. 2d). This suggests that the average displacement of the backbone atoms of the S-protein is mainly driven by the conformation of the S2-domain. The impact of the mutation on the domain conformation of the S-protein was largely noticed in S2-domain than the NTD and the RBD. Collectively, the backbone-RMSD and domain-specific RMSD show that the D614G S-protein adopts a distinct conformation, but seems to be skewed towards the open-state conformation more than the wild-type conformation.

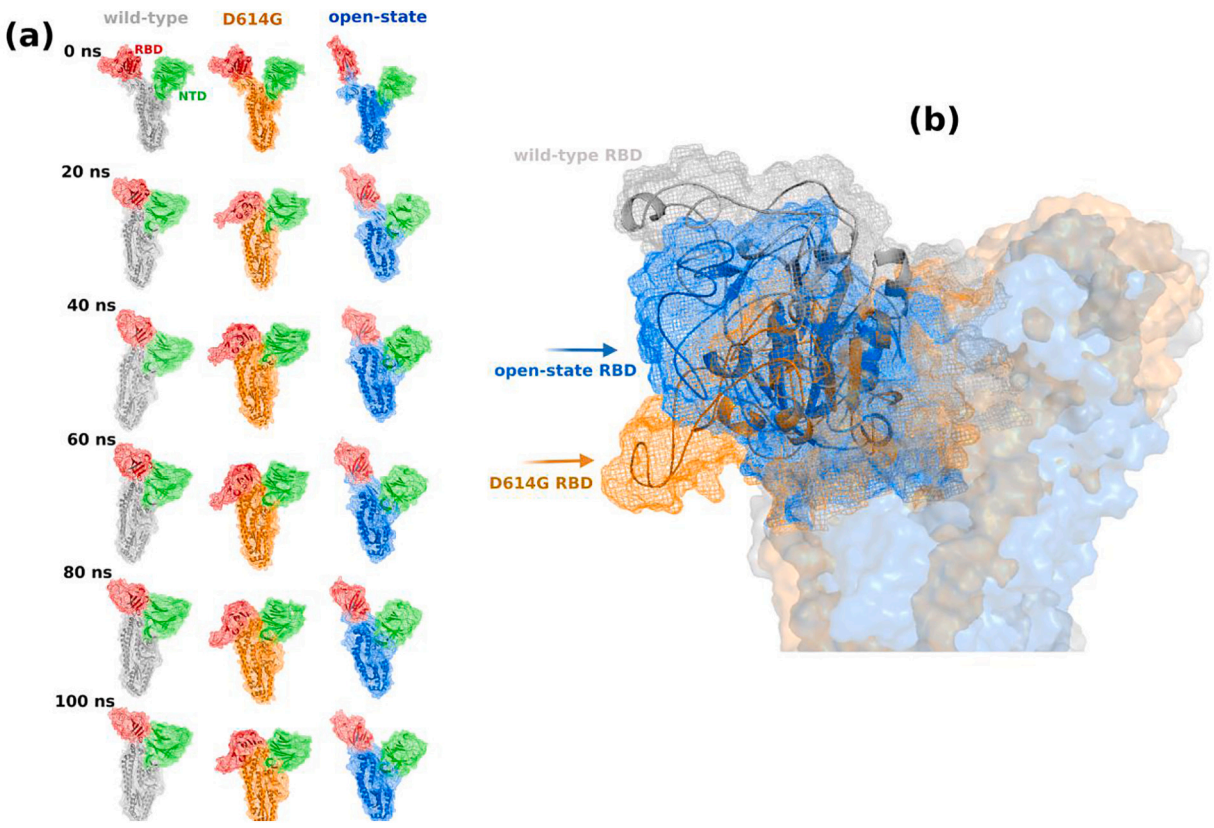

Fig. 4. Molecular view of the protein structures. (a) Snapshots of the structural conformations of the protein systems at different time points of the simulation. The RBD and the NTD are highlighted in red and green, respectively. (**b**) Conformation of the RBD in the wild-type, D614G and open-state S-proteins. The middle structure of the most populated cluster group for each protein was used for structural superposition.

The RMSF indicates the residue-specific flexibility of the protein systems. It can be used to describe the overall structural behaviour of the proteins on a residue-by-residue basis (Dong et al., 2018). Evaluating the residue movement and flexibility would contribute to understanding the structural similarities or differences between the wild-type and D614G S-proteins as well as help in the study of the S-protein interactions with neutralizing antibodies. As shown in Fig. 3, there are notable residue-specific variations in the proteins, mostly affecting the RBD (residue 330–520) and the S2-domain (residue 600–1068). Few regions in the NTD showed huge residue-specific variations in residue flexibility (residue 65–80 and residue 144–153). In general, the open-state NTD has a distinct residue flexibility pattern compared to the wild-type and D614G S-proteins. There were large variations in the RBD residue flexibility for the wild-type and D614G S-protein. The affected regions included residues 330–341, 361–424, 434–463 and 476–518. These amino acids have been characterized as key residues involved in the interaction between

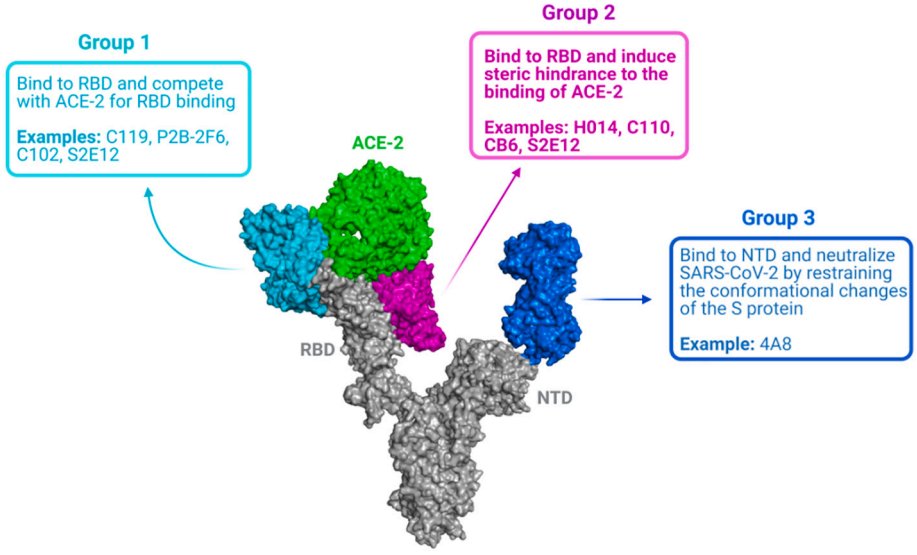

Fig. 5. Classification of SARS-CoV-2 neutralizing antibodies. The neutralizing antibodies are grouped on the basis of their mechanism of neutralization and the domain of binding.

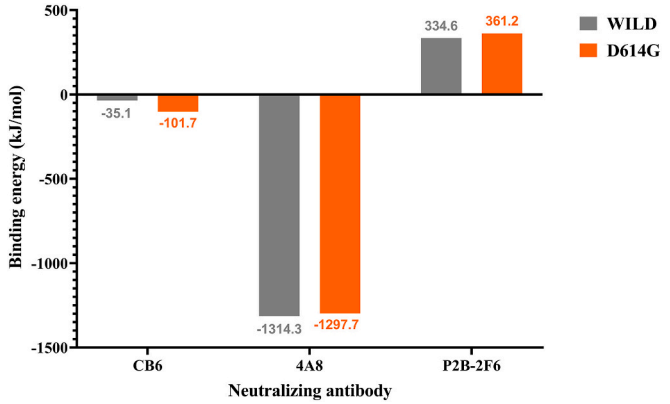

Fig. 6. MM-PBSA binding energy of the complexes.

the RBD and neutralizing antibodies (Lan et al., 2020; Tai et al., 2020; Yi et al., 2020). The flexibility pattern of the RBD residues were also similar in some regions (residue 330–391) of the D614G and open-state S-proteins. Nonetheless, the observed variations in residue flexibility for the D614G RBD may affect the interactions underlying the neutralization of the variant.

Analysis of the simulation trajectories has demonstrated that indeed the D614G S-protein has a distinct structural conformation and residue-specific flexibility variations compared to the wild-type S-protein. The difference in conformational stability was mainly driven by the high displacement of backbone atoms in the S2-domain. We took a closer look at the molecular structures of the trajectories to observe the structures of the RBD and the NTD during the simulation. Molecular structures of the protein systems were extracted from the trajectories every 20 ns. The snapshots of the structures are shown in Fig. 4a. Comparing the RBD of the wild-type and D614G S-proteins shows the mutation affects the structural dynamics of the RBD. Structural superposition of the proteins structures (middle structures of the top cluster groups) also shows that the D614G RBD adopts a conformation similar to the open-state RBD (Fig. 4b).

3.3. Effect of the mutation on the interactions between the S-protein and neutralizing antibodies

Analysis of the molecular dynamics simulation trajectories and structures have shown that the D614G S-protein has distinct structural conformation and residue-specific variations in residue flexibility compared to the wild-type S-protein. Several regions in the NTD, RBD and S2-domain have shown significant variations in the residue flexibility. These differences may affect the interactions between the D614G S-protein and neutralizing antibody (nAb).

The antibodies that mediate neutralization of the virus bind to either the RBD (in most cases) or the NTD of the S-protein to interfere in virus-receptor interactions. We have categorized the neutralizing antibodies into three groups based on the mechanism of neutralization and the domain of binding (Fig. 5). The group 1 nAb bind to the RBD and compete with ACE-2 for RBD binding (Ju et al., 2020), the group 2 nAb bind to the RBD and induce a steric hindrance to the binding of ACE-2 (Shi et al., 2020), and the group, 3 nAb bind to the NTD, neutralize SARS-CoV-2 by restraining the conformational changes of the S protein (Chi et al., 2020). The antibodies CB6, P2B—2F6, and 4A8 were selected to represent groups 1, 2 and 3, respectively. CB6 has demonstrated efficient SARS-CoV-2 neutralization in vitro and also prevented SARS-CoV-2 infections in rhesus monkey subjects when administered (Shi et al., 2020). CB6 recognizes RBD epitopes that overlap with the binding site of ACE-2, thereby inducing steric clash to the binding of ACE-2 (Shi et al., 2020). P2B-2F6 directly competes with the RBD for the ACE-2 receptor with very similar binding affinities (Ju et al., 2020). 4A8 showed high neutralizing activity against SARS-CoV-2 while binding to the NTD (Chi et al., 2020). The very plausible mechanism of neutralization is to block conformational changes of the S-protein (Chi et al., 2020).

To investigate the potential impact of the mutation on the interactions between the antibodies and the S-protein, we performed 15 ns simulations of the molecular systems in triplicates. The trajectories were joined together and were used to calculate the binding energy and residue-specific interaction energies between the S-protein and the neutralizing antibodies. The molecular systems were composed of the selected neutralizing antibody (Fab domain) bound to the RBD or NTD of the wild-type and D614G S-proteins. The overall binding energies of the various interactions are shown in Fig. 6. The binding energy of the wild-CB6 complex and D614G-CB6 complex were − 35.1 kJ/mol and − 101.7 kJ/mol, respectively. The wild-4A8 complex and D614G-4A8 complex showed binding energy of −1314.3 kJ/mol and − 1297.7 kJ/mol, respectively. The binding energy of the wild-P2B-2F6 complex and D614G-P2B-2F6 complex were − 35.1 kJ/mol and − 101.7 kJ/mol, respectively. According to the estimated binding energies, the D614G S-protein interacted better with the CB6 than the wild wild-type S-protein. However, the interactions between the S-protein and 4A8 or P2B-2F6 were relatively similar for the wild-type and D614G variant.

The decomposition of the binding energy into separate energy terms shows that the electrostatic energy term is the major source of the varying binding energy observed for the interactions with the CB6 (Table 1). The electrostatic energy contribution towards the complexation of CB6 was −443.078 kJ/mol for the wild-type S-protein and − 815.532 kJ/mol for the D614G S-protein. Moreover, there was a large difference in polar solvation energy for the wild-CB6 (1095.091 kJ/mol) and D614G-CB6 (1434.865 kJ/mol) complexes. The electrostatic energy contribution emanates from non-bonded interactions involving charged residues at the interacting interface (Kumari et al., 2014). The polar solvation energy term is the electrostatic contribution to the free energy of solvation (Kumari et al., 2014), thus is related to the electrostatic energy term. Estimating the MM-PBSA binding energy has shown that the D614G S-protein has better interactions with the CB6 than the wild-type S-protein, but comparable interactions with 4A8 and P2B—2F6. The difference in interaction with CB6 was driven by a large difference in the electrostatic energy contribution, which involves the interactions between charged amino acid residues and the interacting interface.

We have further decomposed the binding energy based on residual contributions in order to identify the differences in residue contributions to the binding energy. The favorable energy contributions from the residues towards the binding of the neutralizing antibodies are shown in Fig. 7. Concerning the interactions with CB6, energy contributions for

Table 1
Binding energy decomposition of the interaction between the S-protein and neutralizing antibody.

Neutralizing antibody	van der Waal energy (kJ/mol)	Electrostatic energy (kJ/mol)	Polar solvation energy (kJ/mol)	SASA energy (kJ/mol)	Binding energy (kJ/mol)
WILD-CB6	−624.658 ± 55.792	−443.078 ± 52.530	1095.091 ± 100.482	−65.431 ± 4.759	−35.076 ± 19.608
D614G-CB6	−648.187 ± 84.537	−815.532 ± 154.762	1434.865 ± 199.875	-72.836 ± 7.757	−101.690 ± 10.123
WILD-P2B-2F6	−409.078 ± 62.653	109.956 ± 30.520	660.597 ± 86.951	−46.876 ± 5.749	334.599 ± 83.723
D614GP2B-2F6	−437.593 ± 39.293	86.583 ± 48.450	762.659 ± 96.422	−50.424 ± 4.391	361.224 ± 74.702
WILD-4A8	−605.283 ± 116.810	−3390.175 ± 66.739	2727.600 ± 150.329	−76.475 ± 10.112	-1314.333 ± 84.263
D614G-4A8	−551.860 ± 10.155	−3082.352 ± 129.347	2427.77 ± 96.751	−71.272 ± 10.509	−1297.705 ± 81.940

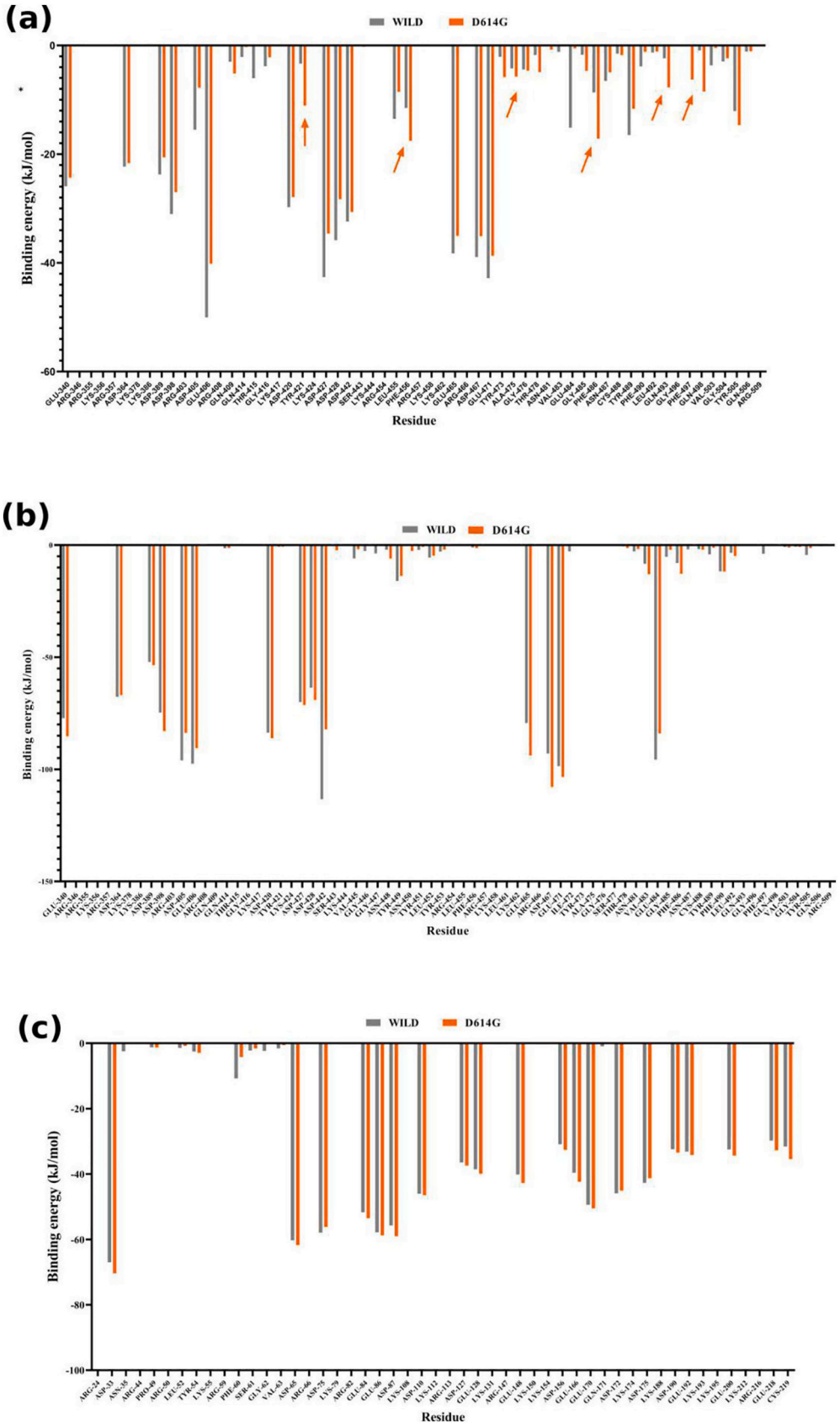

Fig. 7. Energy contributions of S-protein residues during interactions with neutralizing antibodies. Residual energy contributions to interaction between the wild-type or D614G S-protein with (**a**) CB6 (**b**) P2B-2F6 (**c**) 4A8 are shown.

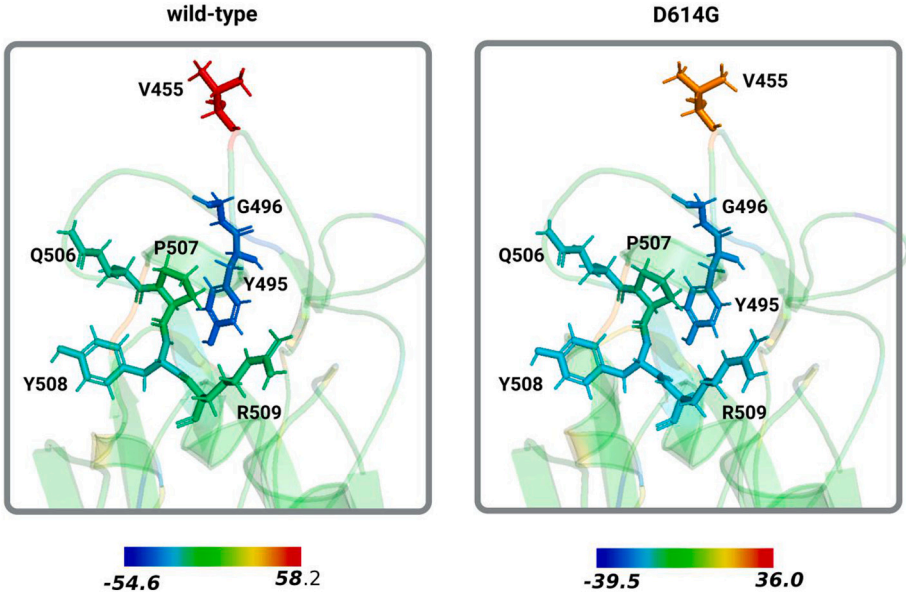

Fig. 8. The mapping of residue energy contribution on the the CB6 interaction interface. The energy contributions are in kJ/mol. The contribution of each residue is shown in colors as represented on the color scale.

some residues varied for the wild-type and D614G S-proteins. These residues (shown in Fig. 7a) contributed higher energies to the D614G-CB6 interaction than the wild-CB6 interaction.

Unlike CB6, the contributions from key residues to the interactions with P2B-2F6 and 4A8 were comparable for the wild-type and D614G S-proteins (Fig. 7b and c), which resulted in the highly similar total binding energies for these interactions. Mapping of the residue energy contributions to the structure of the RBD-CB6 interaction interface revealed further support to the observed variation in residue contributions. The contributions from wild-type S-protein residues ranged from −54.6 to 58.2 kJ/mol and − 39.5 to 36.0 kJ/mol from the D614G S-protein residues. Seven key residues with varying energy contributions to the CB6 interactions were noticed (Fig. 8).

4. Discussion

In this study, we used molecular dynamics simulation to explore the structural conformation of the wild-type and the D614G S-proteins of SARS-CoV-2 and provide a plausible description of the impact the mutation has on the molecular features of interaction with neutralization antibodies. Previous strains of the coronavirus and the current SARS-CoV-2 have demonstrated the selection of mutations as a mechanism of escaping immune responses against them (Li et al., 2020; Sui et al., 2008; Tang et al., 2018; ter Meulen et al., 2006). Moreover, variants that confer resistance to neutralizing antibodies or convalescent plasma may have been selected but are present at low frequencies in SARS-CoV-2 infected populations (Weisblum et al., 2020). The D614G variant emerged around late January to mid-February 2020 and within 1 month, emerged as the dominant circulating strain in Europe and its environs (Isabel et al., 2020; Korber et al., 2020). The variant was characterized by the higher viral load, which is not associated with disease severity (Korber et al., 2020; Volz et al., 2021), higher incorporation into virion (Zhang et al., 2020), and higher cell entry via ACE-2 and TMPRSS2 (Ogawa et al., 2020; Ozono et al., 2021). The results of this study have shed insights into the behaviour of the D614G S-protein at the molecular level and provided a glimpse of the neutralization mechanism of this variant.

The results of this study data show that the D614G S-protein adopts a conformation that is skewed towards the open-state conformation more than the wild-type conformation. Similar observations have been reported previously (Mansbach et al., 2020; Yurkovetskiy et al., 2020b). Our data also shows that there is an allosteric effect to the RBD structural conformation as a result of the D614G mutation. The residue-specific variations in amino acid flexibility and domain-specific RMSD support our claim that the mutation of aspartate to glycine at position 614 in the CTD affects the conformational dynamics of the RBD. Cryo-EM structural studies arrived at a similar conclusion that the mutation to G614 alters the conformation dynamics of the S-protein that demonstrates an allosteric effect on the RBD dynamics (Gobeil et al., 2021).

Analysis of the interaction energies between the S-protein and neutralizing antibodies show that the efficiency of neutralizing activity of the D614G variant is dependent on the neutralizing antibody. In this study, we categorized the neutralizing antibodies into three groups based on the neutralization mechanism and selected one antibody from each group for the analysis. Neutralizing antibodies in group 1 bind to the RBD and compete with ACE-2 for binding site. The antibodies that neutralize by binding to the RBD and inducing steric clashes to the binding of the RBD to ACE-2 were put in group 2. The group 3 antibodies bind to the NTD and neutralize by restraining any conformational changes of the S-protein. The neutralizing antibodies CB6, P2B-2F6 and 4A8 were selected to represent groups 1, 2 and 3, respectively. Unlike P2B-2F6 and 4A8, we noticed a huge difference in the interactions with CB6. The D614G S-protein interacted with the CB6 antibody better than the wild-type. This change in affinity was as a result of large difference in the electrostatic energy contributions. The electrostatic energy term involves interactions between charged amino acids at the interaction interface of the RBD-CB6 complex. There is a possibility that the mutation induces changes in RBD conformational dynamics, thereby exposing otherwise buried residues as previously suggested (Weissman et al., 2021). The RBD also harbors several charged amino acids that are available for interaction with the ACE-2 receptor only in the open-state (Yi et al., 2020).

The results suggest that the mutation may enhance, reduce or not affect the neutralizing interactions depending on the neutralizing antibody. In this study, the mutation reduced the interaction with CB6 but no effect was noticed on the interactions with 4A8 and P2B—2F6. SARS-CoV-2 neutralizing assay data from Chile demonstrated that some samples from individuals exposed to the virus showed enhanced or decreased neutralizing activity against the D614G variant compared to the wild-type (Beltrán-Pavez et al., 2021). In another study, the D614G

variant was more susceptible to neutralization by RBD monoclonal antibodies and convalescent sera from individuals infected with the virus (Weissman et al., 2021). Several studies have reported that there is a similar neutralizing potency of the wild-type and D614G variant when treated with convalescent sera of individuals exposed to the virus (Lee et al., 2021; Yurkovetskiy et al., 2020a, 2020b; Zhang et al., 2020).

In summary, our results show that the D614G S-protein adopts a distinct conformational dynamics, which is skewed towards the open-state conformation more than the wild-type conformation. Residue-specific variation of amino acid flexibility and domain-specific RMSD suggest that the mutation causes an allosteric conformational change in the RBD. Evaluation of the interaction energies between the S-protein and neutralizing antibodies show that the mutation may increase, decrease or not affect the neutralizing interactions depending on the neutralizing antibody.

Credit author statement

Concecptualization; AK, EA.
Data Curation; AK, EA, SOA.
Formal analysis; AK, EA, AAS, AL, SAS, SOA.
Investigation; AK, EA, AAS, AL, SAS, SOA.
Methodology; AK, EA.
Writing - original draft; AK, EA.
Writing - review and editing; AK, EA, AAS, AL, SAS, SOA.

Funding

This research did not receive any specific grant from any funding agency in the public, commercial, or not-for-profit sectors.

Declaration of Competing Interest

The authors declare they have no competing interest.

References

Abraham, M.J., et al., 2015. Gromacs: high performance molecular simulations through multi-level parallelism from laptops to supercomputers. SoftwareX 1–2, 19–25.

Ashkenazy, H., Abadi, S., Martz, E., Chay, O., Mayrose, I., Pupko, T., Ben-Tal, N., 2016. ConSurf 2016: an improved methodology to estimate and visualize evolutionary conservation in macromolecules. Nucleic Acids Res. 44 (W1), W344–W350. https://doi.org/10.1093/nar/gkw408.

Barnes, C.O., West, A.P.J., Huey-Tubman, K.E., Hoffmann, M.A.G., Sharaf, N.G., Hoffman, P.R., Koranda, N., Gristick, H.B., Gaebler, C., Muecksch, F., Lorenzi, J.C.C., Finkin, S., Hägglöf, T., Hurley, A., Millard, K.G., Weisblum, Y., Schmidt, F., Hatziioannou, T., Bieniasz, P.D., Bjorkman, P.J., 2020. Structures of human antibodies bound to SARS-CoV-2 spike reveal common epitopes and recurrent features of antibodies. Cell 182 (4), 828–842 e16. https://doi.org/10.1016/j.cell.2020.06.025.

Beltrán-Pavez, C., Riquelme-Barrios, S., Oyarzún-Arrau, A., Gaete-Argel, A., González-Stegmaier, R., Cereceda-Solis, K., Aguirre, A., Travisany, D., Palma-Vejares, R., Barriga, G.P., Gaggero, A., Martínez-Valdebenito, C., Le Corre, N., Ferrés, M., Balcells, M.E., Fernandez, J., Ramírez, E., Villarroel, F., Valiente-Echeverría, F., Soto-Rifo, R., 2021. Insights into neutralizing antibody responses in individuals exposed to SARS-CoV-2 in Chile. Sci. Adv. 7 (7) https://doi.org/10.1126/sciadv.abe6855.

Chi, X., Yan, R., Zhang, J., Zhang, G., Zhang, Y., Hao, M., Zhang, Z., Fan, P., Dong, Y., Yang, Y., Chen, Z., Guo, Y., Zhang, J., Li, Y., Song, X., Chen, Y., Xia, L., Fu, L., Hou, L., Chen, W., 2020. A neutralizing human antibody binds to the N-terminal domain of the Spike protein of SARS-CoV-2, 655, pp. 650–655. August.

Deller, M.C., Rupp, B., 2015. Models of protein-ligand crystal structures: trust, but verify. J. Comput. Aided Mol. Des. 29, 817–836.

Dong, Y.W., Liao, M.L., Meng, X.L., Somero, G.N., 2018. Structural flexibility and protein adaptation to temperature: molecular dynamics analysis of malate dehydrogenases of marine molluscs. Proc. Natl. Acad. Sci. U. S. A. 115 (6), 1274–1279. https://doi.org/10.1073/pnas.1718910115.

Gobeil, S.M.-C., Janowska, K., McDowell, S., Mansouri, K., Parks, R., Manne, K., Stalls, V., Kopp, M.F., Henderson, R., Edwards, R.J., Haynes, B.F., Acharya, P., 2021. D614G mutation alters SARS-CoV-2 spike conformation and enhances protease cleavage at the S1/S2 junction. Cell Rep. 34 (2), 108630. https://doi.org/10.1016/j.celrep.2020.108630.

Isabel, S., Graña-Miraglia, L., Gutierrez, J.M., Bundalovic-Torma, C., Groves, H.E., Isabel, M.R., Eshaghi, A., Patel, S.N., Gubbay, J.B., Poutanen, T., Guttman, D.S., Poutanen, S.M., 2020. Evolutionary and structural analyses of SARS-CoV-2 D614G spike protein mutation now documented worldwide. Sci. Rep. 10 (1), 14031. https://doi.org/10.1038/s41598-020-70827-z.

Ju, B., Zhang, Q., Ge, J., Wang, R., Sun, J., Ge, X., Yu, J., Shan, S., Zhou, B., Song, S., Tang, X., Yu, J., Lan, J., Yuan, J., Wang, H., Zhao, J., Zhang, S., Wang, Y., Shi, X., Zhang, L., 2020. Human neutralizing antibodies elicited by SARS-CoV-2 infection. Nature 584 (7819), 115–119. https://doi.org/10.1038/s41586-020-2380-z.

Kaushal, N., Gupta, Y., Goyal, M., Khaiboullina, S.F., 2020. Mutational Frequencies of SARS-CoV-2 Genome during the Beginning Months of the Outbreak in USA, pp. 1–16.

Korber, B., Fischer, W.M., Gnanakaran, S., Labranche, C.C., Saphire, E.O., Montefiori, D. C., Korber, B., Fischer, W.M., Gnanakaran, S., Yoon, H., Theiler, J., Abfalterer, W., Partridge, D.G., Evans, C.M., Freeman, T.M., De Silva, T.I., 2020. Article Tracking Changes in SARS-CoV-2 Spike : Evidence that D614G Increases Infectivity of the COVID- ll Tracking Changes in SARS-CoV-2 Spike : Evidence that D614G Increases Infectivity of the COVID-19 Virus, pp. 812–827. https://doi.org/10.1016/j.cell.2020.06.043.

Kumari, R., Kumar, R., Lynn, A., 2014. g_mmpbsa–a GROMACS tool for high-throughput MM-PBSA calculations. J. Chem. Inf. Model. 54 (7), 1951–1962. https://doi.org/10.1021/ci500020m.

Lan, J., Ge, J., Yu, J., Shan, S., Zhou, H., Fan, S., Zhang, Q., 2020. Structure of the SARS-CoV-2 spike receptor-binding domain bound to the ACE2 receptor. Nature 581 (May). https://doi.org/10.1038/s41586-020-2180-5.

Lee, C.Y.-P., Amrun, S.N., Chee, R.S.-L., Goh, Y.S., Mak, T.-M., Octavia, S., Yeo, N.K.-W., Chang, Z.W., Tay, M.Z., Torres-Ruesta, A., Carissimo, G., Poh, C.M., Fong, S.-W., Bei, W., Lee, S., Young, B.E., Tan, S.-Y., Leo, Y.-S., Lye, D.C., Ng, L.F., 2021. Human neutralising antibodies elicited by SARS-CoV-2 non-D614G variants offer cross-protection against the SARS-CoV-2 D614G variant. Clinical & Translational Immunology 10 (2), e1241. https://doi.org/10.1002/cti2.1241.

Li, Q., Wu, J., Nie, J., Zhang, L., Hao, H., Liu, S., Zhao, C., Zhang, Q., Liu, H., Nie, L., Qin, H., Wang, M., Lu, Q., Li, X., Sun, Q., Liu, J., Zhang, L., Li, X., Huang, W., Wang, Y., 2020. The impact of mutations in SARS-CoV-2 spike on viral infectivity and antigenicity. Cell 182 (5), 1284–1294 e9. https://doi.org/10.1016/j.cell.2020.07.012.

Liu, J.W., et al., 2017. On the relationship between residue structural environment and sequence conservation in proteins. Proteins 85, 1713–1723.

Mansbach, R.A., Montefiori, D.C., Gnanakaran, S., Biology, T., Alamos, L., Alamos, L., 2020. The SARS-CoV-2 Spike Variant D614G Favors an Open Conformational State.

Ngoi, J.M., Quashie, P.K., Morang'a, C.M., Bonney, J.H., Amuzu, D.S., Kumordjie, S., Asante, I.A., Bonney, E.Y., Eshun, M., Boatemaa, L., Magnusen, V., Kotey, E.N., Ndam, N.T., Tei-Maya, F., Arjarquah, A.K., Obodai, E., Otchere, I.D., Bediako, Y., Mutungi, J.K., Awandare, G.A., 2020. Genomic analysis of SARS-CoV-2 reveals local viral evolution in Ghana. Experimental Biology and Medicine (Maywood, N.J.). https://doi.org/10.1177/1535370220975351, 1535370220975351.

Ogawa, J., Zhu, W., Tonnu, N., Singer, O., Hunter, T., Ryan, A.L., Pao, G.M., 2020. The D614G mutation in the SARS-CoV2 Spike protein increases infectivity in an ACE2 receptor dependent manner. 90033(4).

Ozono, S., Zhang, Y., Ode, H., Sano, K., Tan, T.S., Imai, K., Miyoshi, K., Kishigami, S., Ueno, T., Iwatani, Y., Suzuki, T., Tokunaga, K., 2021. SARS-CoV-2 D614G spike mutation increases entry efficiency with enhanced ACE2-binding affinity. Nat. Commun. 12 (1), 848. https://doi.org/10.1038/s41467-021-21118-2.

Piccoli, L., Park, Y.-J., Tortorici, M.A., Czudnochowski, N., Walls, A.C., Beltramello, M., Silacci-Fregni, C., Pinto, D., Rosen, L.E., Bowen, J.E., Acton, O.J., Jaconi, S., Guarino, B., Minola, A., Zatta, F., Sprugasci, N., Bassi, J., Peter, A., De Marco, A., Veesler, D., 2020. Mapping neutralizing and Immunodominant sites on the SARS-CoV-2 spike receptor-binding domain by structure-guided high-resolution serology. Cell 183 (4), 1024–1042 e21. https://doi.org/10.1016/j.cell.2020.09.037.

Shi, R., Shan, C., Duan, X., Chen, Z., Liu, P., Song, J., Song, T., Bi, X., Han, C., Wu, L., Gao, G., Hu, X., Zhang, Y., Tong, Z., Huang, W., Liu, W.J., Wu, G., Zhang, B., Wang, L., Yan, J., 2020. A human neutralizing antibody targets the receptor-binding site of SARS-CoV-2. Nature 584 (August). https://doi.org/10.1038/s41586-020-2381-y.

Sui, J., Aird, D.R., Tamin, A., Murakami, A., Yan, M., Yammanuru, A., Jing, H., Kan, B., Liu, X., Zhu, Q., Yuan, Q.A., Adams, G.P., Bellini, W.J., Xu, J., Anderson, L.J., Marasco, W.A., 2008 Nov. Broadening of neutralization activity to directly block a dominant antibody-driven SARS-coronavirus evolution pathway. PLoS Pathog 4 (11), e1000197. https://doi.org/10.1371/journal.ppat.1000197. Epub 2008 Nov 7. PMID: 18989460; PMCID: PMC2572002.

Tai, W., He, L., Zhang, X., Pu, J., Voronin, D., 2020. Characterization of the receptor-binding domain (RBD) of 2019 novel coronavirus : implication for development of RBD protein as a viral attachment inhibitor and vaccine. Cellular & Molecular Immunology (March). https://doi.org/10.1038/s41423-020-0400-4.

ter Meulen, J., van den Brink, E.N., Poon, L.L., Marissen, W.E., Leung, C.S., Cox, F., Cheung, C.Y., Bakker, A.Q., Bogaards, J.A., van Deventer, E., Preiser, W., Doerr, H. W., Chow, V.T., de Kruif, J., Peiris, J.S., Goudsmit, J., 2006 Jul. Human monoclonal antibody combination against SARS coronavirus: synergy and coverage of escape mutants. PLoS Med 3 (7), e237. https://doi.org/10.1371/journal.pmed.0030237. PMID: 16796401; PMCID: PMC1483912.

Vanommeslaeghe, K., Hatcher, E., Acharya, C., Kundu, S., Zhong, S., Shim, J., Darian, E., Guvench, O., Lopes, P., Vorobyov, I., MacKerell Jr., A.D., 2010. CHARMM.pdf. J. Comput. Chem. 31 (4), 671–690. https://doi.org/10.1002/jcc.21367.CHARMM.

Volz, E., Hill, V., McCrone, J.T., Price, A., Jorgensen, D., O'Toole, Á., Southgate, J., Johnson, R., Jackson, B., Nascimento, F.F., Rey, S.M., Nicholls, S.M., Colquhoun, R. M., da Silva Filipe, A., Shepherd, J., Pascall, D.J., Shah, R., Jesudason, N., Li, K., Connor, T.R., 2021. Evaluating the effects of SARS-CoV-2 spike mutation D614G on transmissibility and pathogenicity. Cell 184 (1), 64–75 e11. https://doi.org/10.1016/j.cell.2020.11.020.

Weisblum, Y., Schmidt, F., Zhang, F., DaSilva, J., Poston, D., Lorenzi, J.C., Muecksch, F., Rutkowska, M., Hoffmann, H.-H., Michailidis, E., Gaebler, C., Agudelo, M., Cho, A., Wang, Z., Gazumyan, A., Cipolla, M., Luchsinger, L., Hillyer, C.D., Caskey, M., Bieniasz, P.D., 2020. Escape from neutralizing antibodies by SARS-CoV-2 spike protein variants. ELife 9. https://doi.org/10.7554/eLife.61312.

Weissman, D., Alameh, M.-G., de Silva, T., Collini, P., Hornsby, H., Brown, R., LaBranche, C.C., Edwards, R.J., Sutherland, L., Santra, S., Mansouri, K., Gobeil, S., McDanal, C., Pardi, N., Hengartner, N., Lin, P.J.C., Tam, Y., Shaw, P.A., Lewis, M.G., Montefiori, D.C., 2021. D614G spike mutation increases SARS CoV-2 susceptibility to neutralization. Cell Host & Microbe 29 (1), 23–31 e4. https://doi.org/10.1016/j.chom.2020.11.012.

Yi, C., Sun, X., Ye, J., Ding, L., Liu, M., Yang, Z., Lu, X., Zhang, Y., 2020. Key residues of the receptor binding motif in the spike protein of SARS-CoV-2 that interact with ACE2 and neutralizing antibodies. Cellular & Molecular Immunology (May). https://doi.org/10.1038/s41423-020-0458-z.

Yuan, S., Chan, H.C.S., Hu, Z., 2017. Using PyMOL as a platform for computational drug design. Wiley Interdisciplinary Reviews: Computational Molecular Science 7 (2), 1–10. https://doi.org/10.1002/wcms.1298.

Yurkovetskiy, L., Pascal, K.E., Tomkins-tinch, C., Nyalile, T., Wang, Y., Baum, A., Diehl, W.E., Carbone, C., Veinotte, K., Egri, S.B., Stephen, F., 2020a. SARS-CoV-2 Spike Protein Variant D614G Increases Infectivity and Retains Sensitivity to Antibodies that Target the Receptor Binding Domain.

Yurkovetskiy, L., Wang, X., Pascal, K.E., Tomkins-Tinch, C., Nyalile, T.P., Wang, Y., Baum, A., Diehl, W.E., Dauphin, A., Carbone, C., Veinotte, K., Egri, S.B., Schaffner, S. F., Lemieux, J.E., Munro, J.B., Rafique, A., Barve, A., Sabeti, P.C., Kyratsous, C.A., Luban, J., 2020b. Structural and functional analysis of the D614G SARS-CoV-2 spike protein variant. Cell 183 (3), 739–751 e8. https://doi.org/10.1016/j.cell.2020.09.032.

Zhang, L., Jackson, C.B., Mou, H., Ojha, A., Peng, H., Quinlan, B.D., Rangarajan, E.S., Pan, A., Vanderheiden, A., Suthar, M.S., Li, W., Izard, T., Rader, C., Farzan, M., Choe, H., 2020. SARS-CoV-2 spike-protein D614G mutation increases virion spike density and infectivity. Nat. Commun. 11 (1), 6013. https://doi.org/10.1038/s41467-020-19808-4.